Photons from the early stages of relativistic heavy-ion collisions

L. Oliva,[1,2] M. Ruggieri,[3] S. Plumari,[4,5] F. Scardina,[4,2] G. X. Peng,[3,6] and V. Greco[4,2,3]
[1]*Department of Physics and Astronomy, University of Catania, Via Santa Sofia 64, I-95123 Catania, Italy*
[2]*INFN-Laboratori Nazionali del Sud, Via Santa Sofia 62, I-95123 Catania, Italy*
[3]*College of Physics, University of Chinese Academy of Sciences, Yuquanlu 19A, Beijing 100049, China*
[4]*Department of Physics and Astronomy, University of Catania, Via Santa Sofia 64, I-95125 Catania, Italy*
[5]*INFN, Sezione di Catania, Via Santa Sofia 64, I-95123 Catania, Italy*
[6]*Theoretical Physics Center for Science Facilities, Institute of High Energy Physics, Beijing 100049, China*
(Received 16 March 2017; revised manuscript received 21 June 2017; published 28 July 2017)

We present results about photon-production in relativistic heavy-ion collisions. The main novelty of our study is the calculation of the contribution of the early-stage photons to the photon spectrum. The initial stage is modeled by an ensemble of classical gluon fields which decay to a quark-gluon plasma via the Schwinger mechanism, and the evolution of the system is studied by coupling classical field equations to relativistic kinetic theory; photon production is then computed by including the pertinent collision processes into the collision integral. We find that the contribution of the early-stage photons to the direct photon spectrum is substantial for $p_T \approx 2$ GeV and higher, the exact value depending on the collision energy; therefore, we identify this part of the photon spectrum as the sign of the early stage. Moreover, the amount of photons produced during the early stage is not negligible with respect to those produced by a thermalized quark-gluon plasma: We support the idea that there is no dark age in relativistic heavy-ion collisions.

DOI: 10.1103/PhysRevC.96.014914

I. INTRODUCTION

Photons are important probes of the system produced in relativistic heavy-ion collisions (RHICs), offering a useful way to investigate the preequilibrium stage, the quark-gluon plasma (QGP), and the hadronic phase. As a matter of fact, photons are emitted during the whole lifetime of the system produced by the collisions, and because their mean free path is much larger than the collision volume, they leave the system undisturbed. For this reason it is often said that they bring to the detectors the information about the particular state that has produced them. Photon production in RHICs has been studied extensively in recent years; see Refs. [1–26] and references therein.

In the lifetime of the fireball produced in RHICs it is possible to distinguish among direct photons, namely those arising from collision processes, and decay photons that are instead produced by hadron decays. Direct photons are then mainly split into prompt photons, produced by primordial scatterings among the nucleons, and thermal photons, which instead are produced by a thermalized QGP and hadron gas. Both thermal and prompt photons have been already intensively studied. It should be remarked, however, that the problem of photon production from a thermalized quark-gluon plasma is still not solved completely: As a matter of fact, the most used rate for a thermalized quark-gluon plasma [9] corresponds to a weak coupling limit result (next-to-leading-order corrections to this result exist [19], but lead to at most a 20% shift upwards of the rate); the question of the thermal emission of photons from a strongly coupled plasma, like the one produced by RHICs, has only recently been addressed by means of holographic techniques [17]. Therefore, it is fair to say that the problem is not yet completely understood.

Besides, the study of the photon emission in the early nonequilibrium stage of HICs is still not complete, because only a very small amount of work has been devoted to this subject [11–14,18,21,22]. We aim to fill this gap here, by presenting results about photon production considering preequilibrium photons on the same footing of thermal photons.

Our main theoretical scheme consists of relativistic transport theory coupled to the dynamics of a classical color field that corresponds to the initial gluon-dominated stage and eventually evolves to QGP. This theoretical model has been used to study the evolution of the early stage of RHICs [27,28], giving a picture that agrees qualitatively, and to some extent also quantitatively, with the one obtained by means of classical Yang-Mills calculations for what concerns the evolution of the pressures in the system [29].

Although the initial state is represented by a classical field that mimics that of glasma [30], the decay of the field produces quickly quarks and gluons that scatter and create photons even when the system is not a thermalized QGP. We implement photon production by means of a collision integral; therefore, we do not follow the common strategy used in previous calculations in which one has to assume local thermalization and integrate the rates over the spacetime volume of the fireball. This is the advantage of using relativistic transport theory, which allows us to study photon production also in the early stages where hydrodynamics cannot be properly (or judiciously) applied. Nonetheless, we will see that in the thermal QGP phase the two approaches give nearly identical results.

With respect to previous calculations based on transport theory [11–13], the main novelty that we bring by our study is the clear identification of the contribution of the early stage of RHICs to the direct photon spectrum, looking for both the relative abundance of the photons produced and the momentum region of the photon spectrum that takes the main contribution from the early stage. We will find that the early stage is quite efficient in producing photons; therefore, our results support the absence of a dark age in RHICs. Photons from a thermalizing early stage have been also studied very recently in Ref. [14],

where the bottom-up thermalization scenario of Ref. [31] has been adopted; classical-statistical simulations have shown that bottom-up is the right thermalization scenario [32,33], and it extrapolates to finite couplings quite well [34,35]. Our results agree with the importance of the early-stage photon production in RHICs already highlighted in Ref. [14]; with respect to Ref. [14], our main novelty is to implement photon production by a code based on relativistic transport theory and set up to follow the dynamical evolution of the system produced in RHICs, from the early stage up to the freeze-out, thus allowing a more direct link to the observables of RHICs. In the bottom-up scenario, Bose-Einstein enhancement factors in the collision integral are potentially important owing to large gluon occupation numbers in the initial stage; these have been considered in Ref. [14], while for simplicity we have not included them in our calculations, although within transport theory they can be implemented [36], leaving their inclusion to future works.

Photons from the preequilibrium stage have been studied very recently within another relativistic transport code [18], where a gluon-dominated initial state is considered and quarks are produced by means of inelastic scatterings. The main difference between our work and Ref. [18] is that in the former, quarks and gluons are produced on the same footing by the decay of the initial classical gluon field, which results in a quicker photon production in the early stage. The gluon-dominated initial stage supported in Ref. [18] agrees with the one featured in Refs. [22,26], where it has been also suggested that the delayed quark emission can help to explain the large elliptic flow of photons, in agreement with the analysis of Ref. [4]. Whether the delayed photon emission can really help to understand the photon v_2 puzzle is still an open problem; see Ref. [13] for a review. The problem of the direct photon elliptic flow has been also addressed with other relativistic transport calculations [11]. We will not consider the v_2 of photons in this article because our goal is to discuss the photon production in the preequilibrium stage, a problem that is equally important and still under debate.

The plan of the article is as follows. In Sec. II we review the Abelian flux tube model that we use for the initial condition, as well as our implementation of transport theory and the photon rate that we implement in the collision integral. In Sec. III we summarize our main results on the photon spectrum and photon abundancy. Finally, in Sec. IV we draw our conclusions.

II. INITIAL CONDITION, ITS EVOLUTION, AND PHOTON PRODUCTION

A. Abelian flux tube model

In this section, we summarize the Abelian flux tube model (AFTm), which we use to define an initial condition in our simulations based on classical gluon fields, as well as the base for the evolution of this field configuration to QGP; see Refs. [27,28,37–54] for details.

The main idea of the AFTm is to replace the glasma with a simpler initial classical color field configuration, in which one considers, in its simplest realization, only the electric part of the color field, which decays into QGP by means of the Schwinger mechanism; the pair creation that occurs locally changes the local dipole moment of the system, creating a displacement current whose backreaction on the evolution of the field is taken into account properly (see below). Besides, it is assumed that the classical field equations are Abelian; namely, the covariant derivatives in the QCD field equations are replaced with ordinary derivatives. We would like to observe, however, that even if the model is named Abelian, such nomenclature simply refers to the fact that in the evolution equation for the classical field, self-interaction terms coming from nonvanishing structure constants of the color gauge group are neglected [53]. However, interactions among the classical field and gluons are still present in this calculations, thanks both to the Schwinger effect which produces charged gluons and to conduction currents which affect the evolution of the field; see the next section for more details. It would be certainly interesting to include the effects of a magnetic color field as well as of the non-Abelian terms in the classical equations of motion; the non-Abelian effects have been investigated in Ref. [55] in the SU(2) case. The upgrade of our simulation code to this more realistic initial condition and early-stage dynamics is in progress, and the results will be the subject of forthcoming publications.

In this work, we assume that the initial color electric field is longitudinal, while transverse components of the field develop owing to transverse color currents. Assuming massless quanta, the number of pairs per unit of spacetime and invariant momentum space produced by the decay of the electric field by the Schwinger effect is [27]

$$\frac{dN_{jc}}{d\Gamma} \equiv p_0 \frac{dN_{jc}}{d^4x d^2p_T dp_z} = \mathcal{R}_{jc}(p_T)\delta(p_z)p_0, \tag{1}$$

with

$$\mathcal{R}_{jc}(p_T) = \frac{\mathcal{E}_{jc}}{4\pi^3}\left|\ln\left(1 \pm e^{-\pi p_T^2/\mathcal{E}_{jc}}\right)\right|, \tag{2}$$

the plus (minus) sign corresponding to the creation of a boson (fermion-antifermion) pair. In this equation p_T, p_z refer to each of the two particles created by the tunneling process; $\mathcal{E}_{jc}$ is the effective force which acts on the tunneling pair, and it depends on color and flavor; it can be written as

$$\mathcal{E}_{jc} = (g|Q_{jc}E| - \sigma_j)\theta(g|Q_{jc}E| - \sigma_j), \tag{3}$$

where E stands for the magnitude of the color field and σ_j denotes the string tension depending on the kind of flavor considered. Moreover, $p_0 = \sqrt{p_T^2 + p_z^2}$ corresponds to the single-particle kinetic energy.

The Q_{jc} are color-flavor charges which, in the case of quarks, correspond to the eigenvalues of the T_3 operator:

$$Q_{j1} = \tfrac{1}{2}, \quad Q_{j2} = -\tfrac{1}{2}, \quad Q_{j3} = 0, \quad j = 1, N_f; \tag{4}$$

for antiquarks, corresponding to negative values of j, the color-flavor charges are just minus the corresponding charges for quarks. Finally, for gluons (which in our notation correspond to $j = 0$) the charges are obtained by building gluons up as the octet of the $3 \otimes \bar{3}$ in color space; in particular [28,53],

$$Q_{01} = 1, \quad Q_{02} = \tfrac{1}{2}, \quad Q_{03} = -\tfrac{1}{2}, \tag{5}$$

and $Q_{04} = -Q_{01}$, $Q_{05} = -Q_{02}$, $Q_{06} = -Q_{03}$.

B. Relativistic transport theory

Our calculation scheme is based on the relativistic transport Boltzmann equation, namely,

$$\left(p^\mu \partial_\mu + g\,Q_{jc} F^{\mu\nu} p_\nu \partial_\mu^p\right) f_{jc}(x,p) = \frac{dN_{jc}}{d\Gamma} + \mathcal{C}_{jc}[f], \quad (6)$$

where $f_{jc}(x,p)$ is the distribution function for flavor j and color c, $F^{\mu\nu}$ is the field strength tensor. On the right-hand side we have the source term $dN/d\Gamma$, which describes the creation of quarks, antiquarks, and gluons owing to the decay of the color electric field, and $\mathcal{C}[f]$, which represents the collision integral. Considering only $2 \to 2$ body elastic scatterings, the collision integral can be written as

$$\mathcal{C}[f] = \int \frac{1}{2E_1}\frac{d^3p_2}{2E_2(2\pi)^3}\frac{d^3p_{1'}}{2E_{1'}(2\pi)^3}\frac{d^3p_2'}{2E_2'(2\pi)^3} \times (f_{1'}f_{2'} - f_1 f_2)|\mathcal{M}|^2 \delta^4(p_1 + p_2 - p_{1'} - p_{2'}), \quad (7)$$

where we omit flavor and color indices for simplicity, $\mathcal{M}$ is the transition matrix for the elastic process linked to the differential cross section through $|\mathcal{M}|^2 = 16\pi s^2 d\sigma/dt$, s being the Mandelstam variable. In our simulations we solve numerically Eq. (6) using the test particles method, and the collision integral is computed using Monte Carlo methods based on the stochastic interpretation of transition amplitude [56–64].

The evolution of the electric color field is given by

$$\nabla \cdot \boldsymbol{E} = \rho, \quad \frac{\partial \boldsymbol{E}}{\partial t} = -\boldsymbol{j}, \quad (8)$$

where ρ corresponds to the color charge density,

$$\rho = g \sum_{j,c} Q_{jc} \int d^3\boldsymbol{p}\, f_{jc}(p), \quad (9)$$

with j,c standing for flavor and color, respectively; the sum in the above equation runs over quarks, antiquarks, and gluons. However, $\boldsymbol{j}$ corresponds to the color electric current which is given by the sum of two contributions; that is,

$$j = j_M + j_D. \quad (10)$$

Here j_M is a colored generalization of the usual electric current density, which in a continuum notation is given by

$$j_M^\mu = g \sum_{j,c} Q_{jc} \int \frac{d^3\boldsymbol{p}}{p_0} p^\mu f_{jc}(p). \quad (11)$$

The term j_D is called the displacement current, arising from the change in time of the dipole moment of the medium induced by pairs pop-up via the Schwinger mechanism in the same way a time variation of the local dipole moment in a medium gives rise to a change in the local electric field [65]. We can write [27]

$$j_D = \sum_{j=0}^{N_f}\sum_{c=1}^{3} \int \frac{d^3\boldsymbol{p}}{p_0}\frac{dN_{jc}}{d\Gamma}\frac{2p_T}{E}, \quad (12)$$

where N_f corresponds to the number of flavors in the calculation. The color charge and current densities depend on the particle distribution function: Hence, they link the field equations (8) to the kinetic equation (6). We solve self-consistently the field and kinetic equations, taking into account the backreaction of particle production and propagation on the color field.

At variance with the standard use of transport theory, in which one fixes a set of microscopic processes into the collision integral, we have developed an approach that fixes the total cross section to have the wanted η/s of the system. By means of this scheme we are able to use the Boltzmann equation to simulate the dynamical evolution of a fluid with specified shear viscosity, in analogy to what is done within hydrodynamical simulations [66–68].

We use the Chapman-Enskog [69] approach to relate shear viscosity to temperature, cross section, and density, which is in agreement with Green-Kubo correlator results [62]. Therefore, we fix η/s and compute the pertinent total cross section by means of the relation

$$\sigma_{\rm tot} = \frac{1}{5}\frac{T}{\rho\, g(a)}\frac{1}{\eta/s}, \quad (13)$$

which is valid for a generic differential cross section $d\sigma/dt \sim \alpha_s^2/(t - m_D^2)^2$, as proved in Eq. [62]. In the above equation $a = m_D/2T$, with m_D the screening mass regulating the angular dependence of the cross section, while

$$g(a) = \frac{1}{50}\int dy\, y^6 \left[\left(y^2 + \frac{1}{3}\right)K_3(2y) - yK_2(2y)\right] h\left(\frac{a^2}{y^2}\right), \quad (14)$$

where K_n is the Bessel function and the function h relates the transport cross section to the total one $\sigma_{\rm tr}(s) = \sigma_{\rm tot}\, h(m_D^2/s)$, being $h(\zeta) = 4\zeta(1+\zeta)[(2\zeta+1)\ln(1+1/\zeta) - 2]$. The $g(a)$ is the proper function accounting for the correct relaxation time $\tau_\eta^{-1} = g(a)\sigma_{\rm tot}\rho$ associated with the shear viscosity transport coefficient. For isotropic cross section, i.e., $m_D \to \infty$, the function $g(a)$ is equal to $2/3$ and Eq. (13) reduces to the relaxation time approximation with $\tau_\eta^{-1} = \tau_{\rm tr}^{-1} = \sigma_{tr}\rho$, while for finite value of m_D, which means anisotropic scatterings, $g(a) < 2/3$. We notice that, in the regime where viscous hydrodynamics applies, the specific microscopic details of the cross section are irrelevant, and our approach is an effective way to employ transport theory to simulate a fluid at a given η/s.

C. Photon production rate

In this study, we implement photon production by adding the $2 \to 2$ standard processes of Compton scattering and quark-antiquark annihilation in the collision integral; see Fig. 1. The differential cross sections for the processes are given by

$$\frac{d\sigma^{\rm Compton}}{dt} = -\frac{\pi\alpha\alpha_s}{3s^2}\frac{u^2+s^2}{us}, \quad (15)$$

$$\frac{d\sigma^{\rm annihil}}{dt} = \frac{8\pi\alpha\alpha_s}{9s^2}\frac{u^2+t^2}{ut}, \quad (16)$$

where s,t,u represent the standard Mandelstam variables. In these equations α_s corresponds to the strong coupling, which

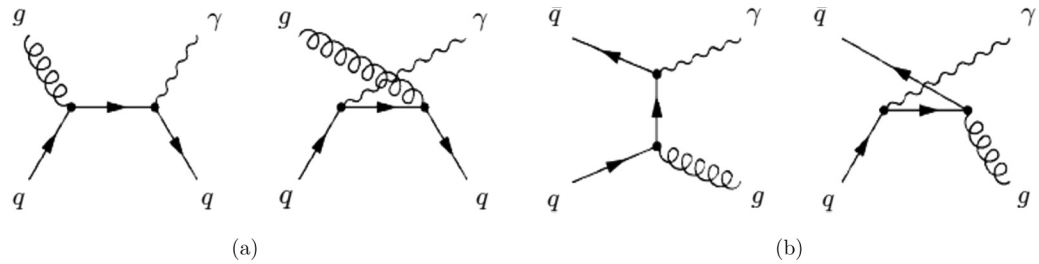

FIG. 1. Microscopic processes implemented in the collision integral: (a) Compton scattering; (b) pair annihilation.

we take running according to the one-loop QCD β function, the sliding scale being the local temperature of the fluid. The photon production rate that would result by considering only the processes in Fig. 1 has been computed in Refs. [6–8]; however, it is well known that the infrared enhancement of $2 \to 3$ processes is important and makes these processes as important as the $2 \to 2$ ones, although these processes would appear to be suppressed by a naive coupling power counting [9]. The $2 \to 3$ processes lead to an increase of the scattering rate with respect to the one obtained considering the $2 \to 2$ processes only: To take into account this fact, at the same time avoiding the difficult implementation of the radiative processes in the collision integral, we follow a very simple strategy, namely we multiply the differential cross sections in Eqs. (15) and (16) by a temperature-dependent overall factor that allows us to reproduce the Arnold-Moore-Yaffe (AMY) production rate [9] at a given temperature. Within this implementation, we are sure that whenever the cell of the fluid is in local equilibrium at a temperature T, the photon spectrum produced by that cell in our code is in fair agreement with the one implemented in calculations based on hydro. Therefore, what we implement in the collision integral are the cross sections

$$\frac{d\sigma^{\text{Compton}}}{dt} = -\Phi(T)\frac{\pi\alpha\alpha_s}{3s^2}\frac{u^2+s^2}{us}, \tag{17}$$

$$\frac{d\sigma^{\text{annihil}}}{dt} = \Phi(T)\frac{8\pi\alpha\alpha_s}{9s^2}\frac{u^2+t^2}{ut}, \tag{18}$$

where $\Phi(T)$ is fixed by hand at the effective local temperature, $T = E/3N$, to reproduce the AMY rate, (see below); here E is the energy of a given cell, and N denotes the total number of particles in that cell. The effective local temperature coincides with the actual temperature when the system is in local equilibrium; however, when the system is out of equilibrium, we assume that the cross sections are still given by Eqs. (17) and (18), and Φ is computed at the scale $T = E/3N$. We notice that for large values of the effective temperature $\Phi \approx 1$, which means that for such large values of the energy density, of the order of those expected in the initial stage, the cross sections implemented in the collision integral are unaffected by this function, and the latter can be considered just as a tool to reproduce the AMY rate when the system is in the equilibrated QGP phase. The multiplicative function Φ does not depend on momenta: As we will show below, this simple choice is enough to obtain a photon production rate that is in fair agreement with AMY in a quite broad range of temperature and photon momentum. A plot of $\Phi(T)$ is shown in Fig. 2.

At this point it is important to clarify that, differently from the previous studies based on hydro, we do not need to integrate the production rate over the spacetime volume of the system to obtain the photon spectrum. As a matter of fact, what we do is to implement photon production in the collision integral, by means of the microscopic cross sections in Eqs. (17) and (18). In this way, we can follow photon production consistently since the very first moments after the collision, namely as soon as the classical color fields decay and produce quarks and gluons, regardless of the fact that the system is in local equilibrium or not.

In Fig. 3 we plot the photon production rate that we implement in the collision integral for three different temperatures: Squares correspond to our rate, obtained by introducing a temperature-dependent multiplicative factor in the $2 \to 2$ process rates to increase the photon production rate, while dashed data stand for the AMY rates computed at the same temperature. We find that our procedure, although rough, reproduces the AMY rates fairly well in the temperature range that is relevant for the RHICs.

III. RESULTS

A. Setup of the initial condition and QGP evolution

In this section we discuss how we set up the initial classical field. We assume a longitudinal direction boost invariant chromoelectric field at the initial time and with a smooth profile in the transverse plane that mimics a standard Glauber-type

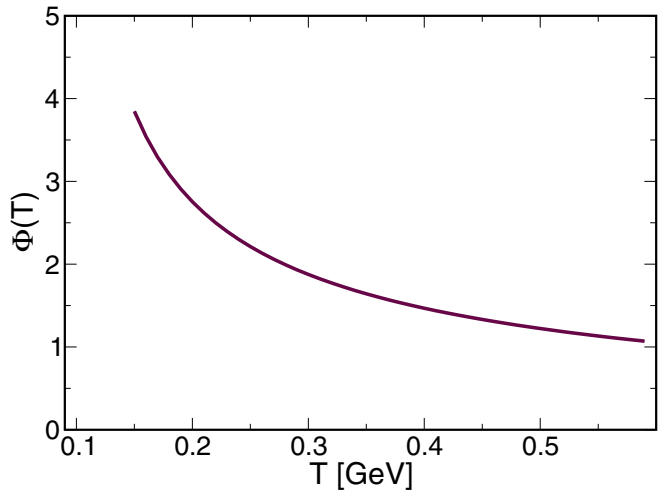

FIG. 2. Function $\Phi(T)$ appearing in Eqs. (17) and (18) versus the effective temperature $T = E/3N$.

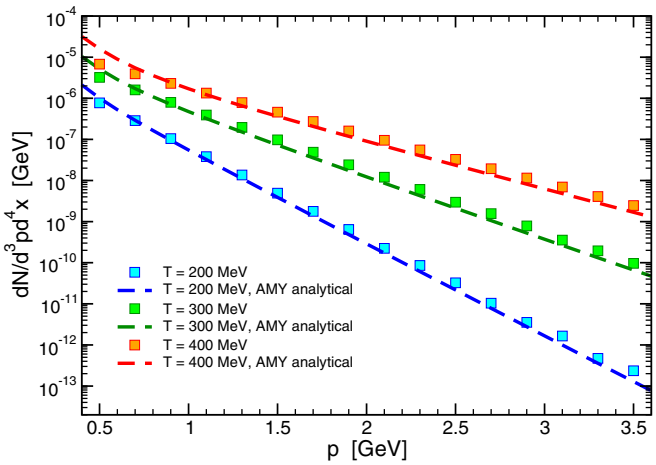

FIG. 3. Photon production rate for several values of the temperature. Dashed lines correspond to the AMY rate at a given temperature, while squares represent the rate implemented in our collision integral.

distribution, namely,

$$E_z^0(\boldsymbol{x}_T) = E_{\max}^0[\alpha\rho_{\rm coll}(\boldsymbol{x}_T) + (1-\alpha)\,\rho_{\rm part}(\boldsymbol{x}_T)], \qquad (19)$$

where $\alpha \leqslant 1$, $\boldsymbol{x}_T$ denotes the transverse plane coordinate, and $\rho_{\rm coll}, \rho_{\rm part}$ correspond to the density of binary collisions and participants in the transverse plane respectively, both being normalized to one. In Eq. (19) two free parameters appear, namely the peak value of the magnitude of the electric field $E_{\max}^0$ and the relative abundance of binary and participant collisions α. These parameters are fixed to match a standard Glauber initialization: In particular, for collisions at RHIC energy we impose that at $t = 0.6$ fm/c, corresponding to a standard initialization time for calculations with the Glauber model, and that the eccentricity of the system within the AFTm is equal to the eccentricity obtained within the Glauber model with the same impact parameter, and we require that the total numbers of particles produced by the two initializations are the same; for collisions at LHC energy we perform the same tuning, by requiring that the eccentricity and the total multiplicity in the two initializations coincide at $t = 0.3$ fm/c. Numerical values of the parameters used in the calculations are in Table I. We decide to implement these constraints on our initial condition because in this way the main differences that we find in the photon spectrum can be related directly to the presence of the preequilibrium evolution in the AFTm that instead is absent in the calculations with the Glauber initialization.

In Fig. 4 we plot the particle numbers of quarks and gluons as functions of time for the case of the AFTm, and we compare these numbers with the ones we use in the calculations with the Glauber initialization. Both panels refer to collisions in the 20%–40% centrality class, for collisions at RHIC in panel (a) and at LHC in panel (b). In the Glauber case the multiplicity is chosen by matching it with the experimental value of the dN/dy for the given centrality class. In both panels of Fig. 4, the thick solid violet lines denote the total number of particles we use in the simulation with the Glauber initialization, which should be compared to the violet circles corresponding to the total number of particles obtained within the AFTm initialization; green thick dashed lines stand for the gluon number in Glauber, while the green squares correspond to gluon number in the AFTm. Finally, the thick red dot-dashed lines correspond to quark + antiquark number in Glauber, while we use the red diamonds to denote the same quantity for the AFTm. For the Glauber calculations we fix the ratio of quark + antiquark over gluon numbers by its value at chemical equilibrium, that for massless particles is independent on temperature and depends only on the degrees of freedom.

TABLE I. Parameters of Eq. (19) corresponding to the collisions examined in this study.

Collision	Centrality	E_0 (GeV^2)	α
Au-Au, 200 AGeV	20–40	3.0	0.7
Pb-Pb, 2.76 ATeV	20–40	6.0	0.85

The total particle numbers in AFTm and Glauber are the same by construction, while the relative abundance of quarks over gluons within the AFTm is not fixed *a priori* but it is a result of the dynamical evolution of the system from the classical gluon field to the QGP via the Schwinger effect. Nevertheless, we find that for the collision at RHIC not only the total particle number, but also the numbers of quarks and gluons match those used in the Glauber model, which are the chemical equilibrated ones. For the case of collisions at LHC we find some mismatch between the two initializations, even if the net difference is not very large. We also notice that within the AFTm, quarks are produced very quickly for collisions at both energies. In fact, starting from the classical color field that represents the gluon-dominated initial state, within 0.4 fm/c quarks are formed, and the relative abundance of quarks with respect to gluons is not very far from the one expected at chemical equilibrium, the latter being represented by the thick lines in Fig. 4. This is a bit different with what has been found in Refs. [18,22,70], where although a gluon-dominated state is considered in the initial condition, quarks are produced solely by inelastic scatterings. This difference is clearly attributable to the fact that within our approach, quarks and gluons are produced statistically on the same footing by the decay of the initial classical gluon field. This difference affects photon production in the preequilibrium stage, as we discuss in the next section.

In Fig. 5 we plot the final spectra for the QGP for the case of collisions at RHIC [panels (a) and (b), respectively] and LHC [panels (c) and (d), respectively]. In the panels, squares correspond to AFTm and circles to Glauber calculations. For both Glauber and AFTm initializations we add also the standard minijets, respectively, for $p_T \geqslant 2$ GeV in the case of RHIC collisions and $p_T \geqslant 3$ GeV for LHC collisions. We notice that final spectra of quarks and gluons in the Glauber calculations fairly agree with the ones of the AFTm, in the cases of both RHIC and LHC collisions.

B. Sign of the early stage on photon spectrum and abundancy

In Fig. 6 we plot the photon spectra at midrapidity for the 20%–40% centrality class. Panel (a) corresponds to collisions at RHIC and panel (b) is the analogous for the LHC case. In

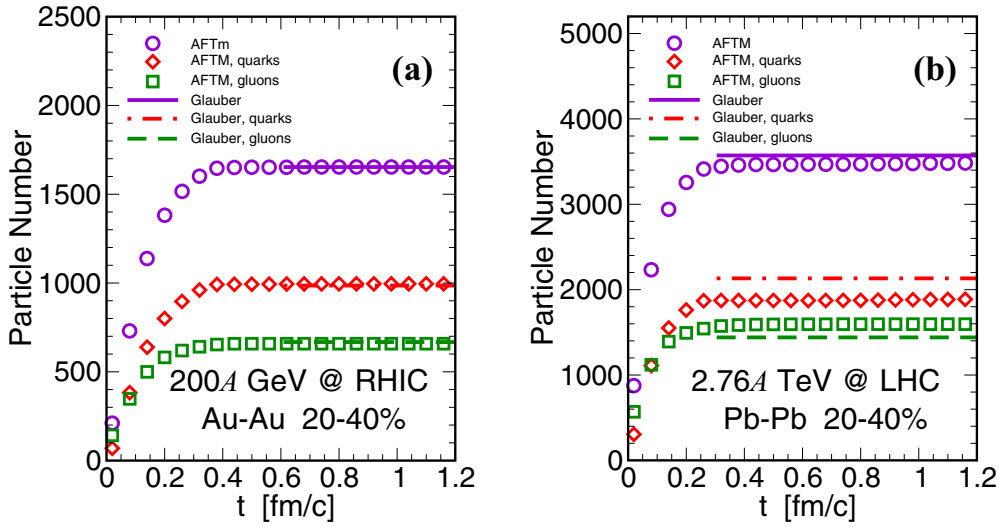

FIG. 4. Quark, gluon, and total particle numbers for the AFTm initialization, compared with the values used in the Glauber initialization. (a) A collision at the RHIC energy; (b) a collision at the LHC energy. Squares, diamonds, and circles correspond to gluons, quarks, and total particle number of the AFTm, respectively. Both panels refer to collisions belonging to the 20%–40% centrality class.

both panels, solid maroon lines correspond to the spectrum obtained within the AFTm, while blue dashed lines stand for the spectrum obtained in simulations with the Glauber initialization. Green dot-dashed lines denote the photon spectrum in the AFTm at $t_0 = 0.6$ fm/c for RHIC, and $t_0 = 0.3$ fm/c for LHC: In both cases we call this the early-stage spectrum. Finally, the orange dotted lines correspond to the difference between the maroon and the green lines, which we call the late-stage spectrum.

Figure 6 corresponds to the main result of our study. First we focus on the RHIC panel because the results for LHC are in qualitative agreement with those for RHIC. We start by noticing that the total number of photons in the case of the AFTm is larger than the one obtained within the Glauber model. This is easy to understand: As a matter of fact, photons in the AFTm are produced as soon as quarks and gluons appear by the decay of the initial classical color field, while in the Glauber calculation this production is delayed up to the initialization time, the latter being usually assumed as the time necessary for the system to reach a local equilibrium in the transverse plane. Integrating the photon spectrum over transverse momentum and rapidity, we find that for the collisions at RHIC the photon abundancy in the AFTm is approximately 30% higher than that obtained within the Glauber model. This difference, coming from the existence of a dynamics in the preequilibrium stage in the AFTm, shows that preequilibrium photons are important as they give a substantial contribution to the total number of photons produced by the QGP. Stated in other terms, the early stage is quite bright. We have also computed the average temperature of the photon gas in the early stage by means of the inverse slope of the photon spectrum: Because of the preequilibrium dynamics, this quantity remains finite and in agreement with the temperature of the bulk already computed

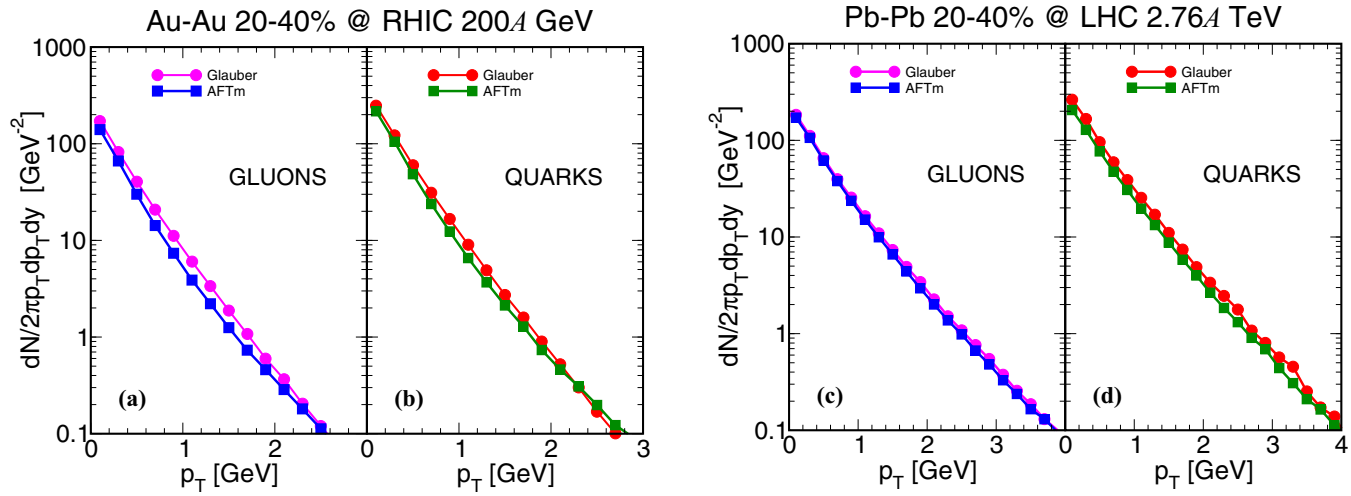

FIG. 5. Final spectra for gluons and quarks at RHIC [panels (a) and (b), respectively] and at LHC [panels (c) and (d), respectively]. In the panels, squares correspond to AFTm and circles to Glauber calculations.

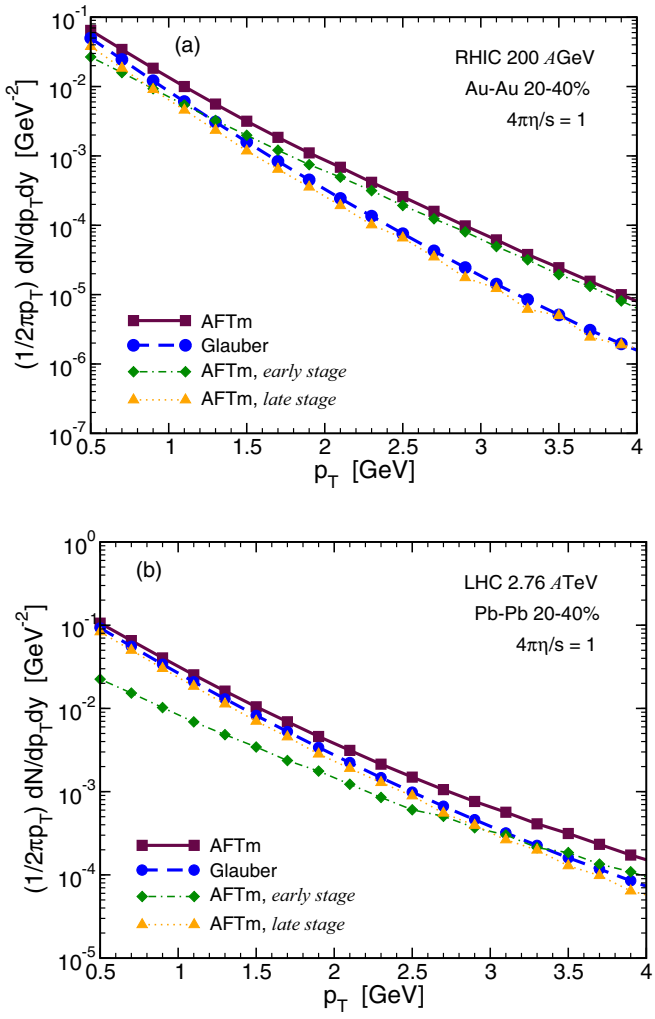

FIG. 6. Photon spectra at midrapidity. Panel (a) corresponds to collisions at RHIC and panel (b) is the analogous for the LHC case. In both panels, solid maroon lines correspond to the spectrum obtained within the AFTm, while blue dashed lines stand for the spectrum obtained in simulations with the Glauber initialization. Green dot-dashed lines denote the photon spectrum in the AFTm at $t_0 = 0.6$ fm/c for RHIC and $t_0 = 0.3$ fm/c for LHC: In both cases we call this the early-stage spectrum. Finally, the orange dotted lines correspond to the difference between the maroon and the green lines, that we call the late-stage spectrum. See the text for more details.

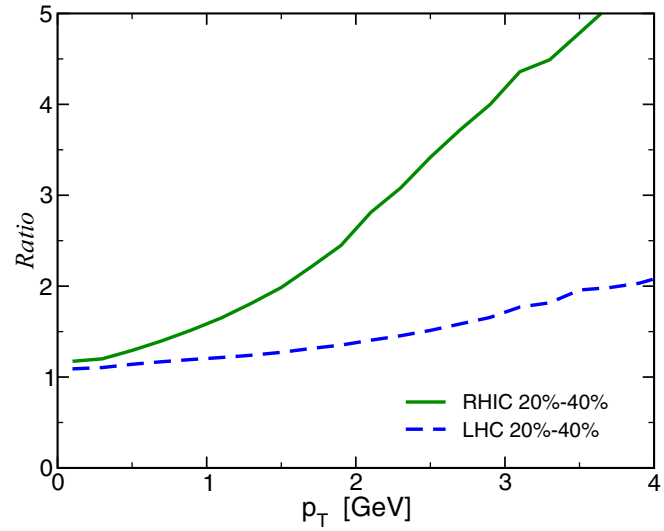

FIG. 7. Ratio of photon spectrum of the AFTm over the one corresponding to the Glauber calculation. The green solid line corresponds to RHIC collision and the blue dashed line to LHC collision.

in Ref. [28], instead of being divergent as it would be if it evolved as $T \propto \tau^{-1/3}$, that is, as in the case of a thermalized system in a one-dimensional expansion.

Introducing a dynamics in the very early stage not only affects the total number of photons produced, but also the shape of the spectrum. In fact, in Fig. 6 we represent by the dotted green line the spectrum obtained at $t = 0.6$ fm/c corresponding to the initialization time of the Glauber calculation; we call this the early-stage contribution to the photon spectrum. We also plot the difference between the final AFTm spectrum and the early-stage ones and represent this difference by the orange dotted line in Fig. 6: We call this the late-stage spectrum, corresponding to the photons produced by the QGP since the initialization time of the Glauber simulation. We notice that the late-stage spectrum agrees with the one obtained within the Glauber calculation: Although the two initial conditions are different, the bulk evolution in the two models match each other perfectly starting from the Glauber initialization time. We would be tempted to name the late-stage spectrum as the equilibrium spectrum; however, a strict distinction between equilibrium and preequilibrium in the AFTm does not apply, because local equilibration in the fireball of the AFTm takes place at different times in different cells, while in the Glauber model the spectrum is already equilibrated in the whole transverse plane at the initialization time.

Comparing the green dot-dashed and the maroon solid lines in Fig. 6, we notice that the most important photon production in the early stage takes place in the momentum region $p_T \gtrsim 1.5$ GeV. We identify the enhancement of the photon spectrum from QGP in this momentum region as the sign of the early-stage photons.

For a matter of comparison, we plot in Fig. 7 the ratio of the final photon spectrum of the AFTm over the one corresponding to the Glauber calculation: The green solid line corresponds to collisions at RHIC and the blue dashed line to LHC collisions. For what concerns Au-Au collisions, we notice the enhancement of photon production within the AFTm for $p_T \gtrsim 1.5$ GeV with respect to the Glauber calculation.

The results for the LHC case, which are summarized in panel (b) of Fig. 6, are qualitatively similar to those already discussed for the RHIC case. For collisions at LHC we find that the domain $p_T \gtrsim 2$ GeV can be identified with the one in which photons are produced in the very early stage. In this case we find that the photon abundancy obtained within the AFTm is about the 20% larger than the one obtained by the Glauber initialization; thus, the effect of the early stage seems to be smaller than the one observed in the case of RHIC collisions. This can be easily understood because for collisions at LHC

the early stage is considerably shorter than the one at RHIC, and also the lifetime of the thermalized QGP at LHC is larger than the one at RHIC; therefore, the net effect of the early stage on photons produced by LHC collisions is naturally smaller than the one that we have measured for RHIC collisions. Therefore, we can summarize the results by stating that the early-stage affects considerably both photon abundancy and the shape of the photon spectrum because of the enhancement of photon production in the intermediate momentum region, namely $p_T \gtrsim 1.5$ GeV at RHIC and $p_T \gtrsim 2$ GeV at LHC.

C. Comparison with PHSD and BAMPS

It is useful to compare our results for the photon spectrum with those obtained by means of other calculations based on relativistic transport. This is done in Fig. 8, where we show the spectrum of photons produced by the quark-gluon plasma within Parton Hadron String Dynamics (PHSD) [11] (blue circles) and Boltzmann Approach for Many Parton Scattering (BAMPS) [18] (red thin solid line, corresponding to a fix coupling, and green dashed line corresponding to a running coupling). In the figure, maroon squares correspond to our result.

The most striking aspect of the results shown in Fig. 8 is that there is a disagreement between PHSD and our results on the one hand and BAMPS on the other hand. However, the reason for this discrepancy is very easy to understand: As a matter of fact, the BAMPS calculation uses a gluon-dominated initial state, but the conversion to quarks is achieved only by the inelastic QCD scatterings, which has the effect of delaying the appearance of quarks and hence of the emission rate of photons. However, within the other two transport calculations quarks and gluons are produced since the beginning because of field decay or string breaking, therefore leading to a larger photon emission of the quark-gluon plasma.

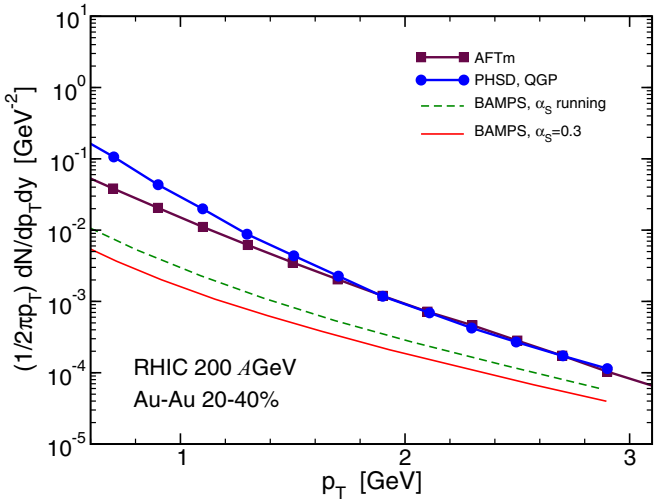

FIG. 8. Photon spectrum produced by the quark-gluon plasma for a RHIC collision, within three different calculations based on relativistic transport: blue circles correspond to PHSD [11], thin red solid line denotes the BAMPS result [18] with a fixed strong coupling, while the dashed green line corresponds to the BAMPS result with a running coupling; finally the maroon squares correspond to our result.

In last analysis, the results in Fig. 8 remind one that there is still a theoretical uncertainty about the production time of the quark-gluon plasma in heavy-ion collisions. One of the consequences of this uncertainty is measurable as the change of the photon abundancy of the quark-gluon plasma.

A direct comparison with experimental data is not very fruitful at this stage of the work, because in our code we miss the hadron gas contribution to photon spectrum. Moreover, the difference between our results and those of other collaborations might be also come in part from the different energy density profiles and not only to the presence and/or absence of preequilibrium photons. A more detailed analysis

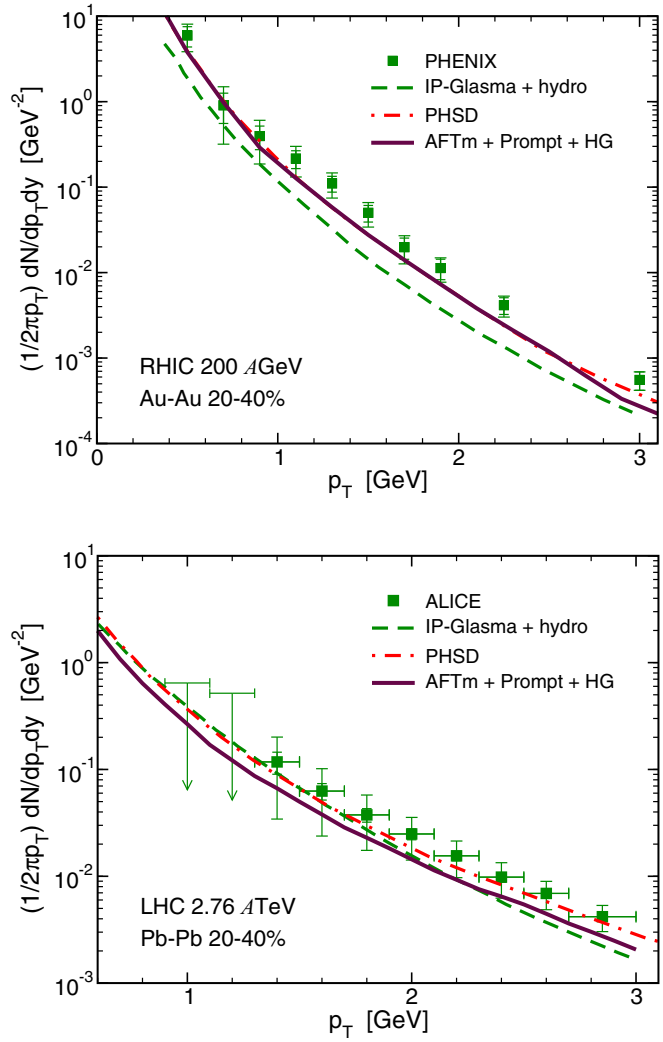

FIG. 9. In the top panel we plot the direct photon spectrum for a RHIC collision. The maroon solid line corresponds to our result for the quark-gluon plasma, to which we have added the prompt photons of Ref. [5] and the hadron gas contribution of Ref. [11]. For comparison, we have shown the IP-glasma + hydro result of Ref. [5], represented by the green dashed line. The red dot-dashed line denotes the PHSD result [11]. Green squares correspond to the experimental data from the PHENIX Collaboration [71]. In the bottom panel we plot the direct photon spectrum for an LHC collision. Line styles and colors are the same as in the top panel. Experimental data are from the ALICE Collaboration [72].

is needed to compare quantitatively the theoretical predictions from the several collaborations. However, just to show that what we find for the quark-gluon plasma spectrum might lead the direct photon spectrum into the right ballpark, we add to our result the prompt and the hadronic photons of Ref. [11].

In the top panel of Fig. 9 we show the result for the direct photon spectrum for a RHIC collision. The maroon solid line corresponds to our result obtained adding the prompt and hadronic photons as explained above. For comparison, we have shown the IP-glasma + hydro result of Ref. [5], represented by the green dashed line. The red dot-dashed line denotes the PHSD result [11]. Experimental data are from the PHENIX Collaboration [71]. We notice that the two transport calculations agree with each other remarkably well and that they tend to lower the tension with experimental data with respect to the IP-glasma + hydro calculation. However, we do not push this result too much because the hadronic contribution should be computed consistently rather than simply added by hand: We plan to consider this problem in the future, while here we prefer to focus on another problem, namely, the photon production from the preequilibrium stage.

In the bottom panel of Fig. 9 we show the result for the direct photon spectrum for an LHC collision. We have once again added to our quark-gluon plasma photons the prompt and hadronic photons computed in Ref. [11]. Experimental data are from the ALICE Collaboration [72]. In this case we find some minor disagreement between the three calculations, which might be a consequence of the fact that for LHC collisions the preequilibrium stage does not affect the direct photon spectrum in a relevant way.

IV. CONCLUSIONS

We have studied the photon production from QGP in RHICs, putting emphasis on the role of the early-stage quark-gluon scatterings on the direct photon spectrum. We have considered a model for the initial conditions in RHICs, based on a classical gluon field mimicking the glasma, beside a mechanism for the conversion of the field to QGP; the dynamics of the QGP has been studied by means of a simulation code based on relativistic transport theory coupled to the classical field dynamics. We have simulated both Au-Au collisions at RHIC energy and Pb-Pb collisions at LHC energy. Our approach, although simplified with respect to the more realistic situation based on glasma and its evolution, allows us to follow consistently the system since the very initial stage up to the freeze-out.

Within our theoretical description, QGP is produced since the very early stage by the decay of the classical gluon field by means of the Schwinger mechanism. As soon as QGP is formed, quarks and gluons scatter, and they can produce photons: Our approach therefore allows us to compute the contribution of the QGP to the photon spectrum, taking into account also the ones produced in the early stages, which have been neglected in previous studies. Although in the collision integral we have considered only the $2 \to 2$ photon production processes, we have artificially modified the scattering matrix of these processes to reproduce the celebrated AMY rate; see Fig. 3. As a consequence, our production rate agrees with the one commonly used in calculations based on hydro.

We have been able to identify a transverse momentum region in which the direct photon spectrum is dominated by the early-stage photons, namely $p_T \gtrsim 1.5$ GeV for collisions at RHIC and $p_T \gtrsim 2$ GeV for collisions at LHC; see Figs. 6 and 7. Moreover, we have found that during the early stages the amount of photons produced is approximately within the 20%–30% of the total amount of photons produced by the QGP. This is a remarkable result considering that the lifetime of the early stage is at most one-tenth of the full QGP lifetime in the fireball: We can conclude that the early stage is quite bright, or stated in other terms, that there is no dark age in RHICs.

We have tried a tentative comparison of our results with the existing RHIC and LHC data about the direct photon spectrum, borrowing the hadronic and prompt photon contributions from existing works [11]. We have found that the net result is in fair agreement with the existing data, as well as with other relativistic transport calculations [11,18]. We have found some disagreement with BAMPS [18], which, however, is clearly understood as arising from both a different initial condition and a different initial early-stage dynamics.

For a matter of simplicity we have not included here the Bose-Einstein enhancement factors in the collision integral, which are potentially relevant in the early stage owing to the large gluon occupation numbers; these have been considered in a recent study [14], and we plan to include them in future works following Ref. [36]. It would also be important to consider initial-state fluctuations that have been proved to be important for photon production [15,16], as well as to gauge the collision integral to the holographic production rate [17] rather than to the AMY rate. These important upgrades of our calculations will be the subject of forthcoming works. We have only considered the direct photon spectrum in this work; owing to the importance of the photon elliptic flow, in relation also to the solution of the direct photon puzzle, we will devote a detailed analysis of this quantity and its comparison to experimental data in future studies.

ACKNOWLEDGMENTS

V.G., S.P., and F.S. would like to acknowledge the ERC-STG funding under a QGPDyn grant. M.R., G.X.P., and V.G. would like to thank the National Natural Science Foundation of China (Grants No. 11575190 and No. 11475110) and the CAS Presents International Fellowship Initiative (Grants No. 2015PM008 and No. 2016VMA063s). We thank Jean-François Paquet, Raju Venugopalan, Zhe Xu, and Moritz Greif for discussions and correspondence.

[1] C. Shen, U. W. Heinz, J. F. Paquet, and C. Gale, Phys. Rev. C **89**, 044910 (2014).

[2] F. M. Liu and K. Werner, J. Phys. G **36**, 035101 (2009).

[3] F. M. Liu, T. Hirano, K. Werner, and Y. Zhu, Phys. Rev. C **79**, 014905 (2009).
[4] F. M. Liu and S. X. Liu, Int. J. Mod. Phys.: Conf. Ser. **29**, 1460230 (2014).
[5] J. F. Paquet *et al.*, Phys. Rev. C **93**, 044906 (2016).
[6] J. I. Kapusta, P. Lichard, and D. Seibert, Phys. Rev. D **44**, 2774 (1991); **47**, 4171(E) (1993).
[7] R. Baier, H. Nakkagawa, A. Niegawa, and K. Redlich, Z. Phys. C **53**, 433 (1992).
[8] R. Baier, H. Nakkagawa, A. Niegawa, and K. Redlich, Phys. Rev. D **45**, 4323 (1992).
[9] P. Arnold, G. D. Moore, and L. G. Yaffe, J. High Energy Phys. 12 (2001) 009.
[10] S. Turbide, R. Rapp, and C. Gale, Phys. Rev. C **69**, 014903 (2004).
[11] O. Linnyk, V. Konchakovski, T. Steinert, W. Cassing, and E. L. Bratkovskaya, Phys. Rev. C **92**, 054914 (2015).
[12] O. Linnyk, W. Cassing, and E. L. Bratkovskaya, Phys. Rev. C **89**, 034908 (2014).
[13] O. Linnyk, E. L. Bratkovskaya, and W. Cassing, Prog. Part. Nucl. Phys. **87**, 50 (2016).
[14] J. Berges, K. Reygers, N. Tanji, and R. Venugopalan, Phys. Rev. C **95**, 054904 (2017).
[15] R. Chatterjee, H. Holopainen, T. Renk, and K. J. Eskola, Phys. Rev. C **85**, 064910 (2012).
[16] R. Chatterjee, H. Holopainen, I. Helenius, T. Renk, and K. J. Eskola, Phys. Rev. C **88**, 034901 (2013).
[17] I. Iatrakis, E. Kiritsis, C. Shen, and D. L. Yang, J. High Energy Phys. 04 (2017) 035.
[18] M. Greif, F. Senzel, H. Kremer, K. Zhou, C. Greiner, and Z. Xu, Phys. Rev. C **95**, 054903 (2017).
[19] J. Ghiglieri, J. Hong, A. Kurkela, E. Lu, G. D. Moore, and D. Teaney, J. High Energy Phys. 05 (2013) 010.
[20] J. Ghiglieri, O. Kaczmarek, M. Laine, and F. Meyer, Phys. Rev. D **94**, 016005 (2016).
[21] M. Chiu, T. K. Hemmick, V. Khachatryan, A. Leonidov, J. Liao, and L. McLerran, Nucl. Phys. A **900**, 16 (2013).
[22] V. Vovchenko *et al.*, PoS BORMIO **2016**, 039 (2016).
[23] A. Ayala, J. D. Castano-Yepes, C. A. Dominguez, and L. A. Hernandez, EPJ Web Conf. **141**, 02007 (2017).
[24] F.-M. Liu, S.-X. Liu, and K. Werner, arXiv:1512.08833.
[25] S.-X. Liu, F.-M. Liu, K. Werner, and M. Yue, arXiv:1607.02572.
[26] F.-M. Liu and S.-X. Liu, Phys. Rev. C **89**, 034906 (2014).
[27] R. Ryblewski and W. Florkowski, Phys. Rev. D **88**, 034028 (2013).
[28] M. Ruggieri, A. Puglisi, L. Oliva, S. Plumari, F. Scardina, and V. Greco, Phys. Rev. C **92**, 064904 (2015).
[29] T. Epelbaum and F. Gelis, Phys. Rev. Lett. **111**, 232301 (2013).
[30] T. Lappi and L. McLerran, Nucl. Phys. A **772**, 200 (2006).
[31] R. Baier, A. H. Mueller, D. Schiff, and D. T. Son, Phys. Lett. B **502**, 51 (2001).
[32] J. Berges, K. Boguslavski, S. Schlichting, and R. Venugopalan, Phys. Rev. D **89**, 074011 (2014).
[33] J. Berges, K. Boguslavski, S. Schlichting, and R. Venugopalan, Phys. Rev. D **89**, 114007 (2014).
[34] A. Kurkela and Y. Zhu, Phys. Rev. Lett. **115**, 182301 (2015).
[35] L. Keegan, A. Kurkela, A. Mazeliauskas, and D. Teaney, J. High Energy Phys. 08 (2016) 171.
[36] F. Scardina, D. Perricone, S. Plumari, M. Ruggieri, and V. Greco, Phys. Rev. C **90**, 054904 (2014).
[37] A. Casher, H. Neuberger, and S. Nussinov, Phys. Rev. D **20**, 179 (1979).
[38] N. K. Glendenning and T. Matsui, Phys. Rev. D **28**, 2890 (1983).
[39] A. Bialas and W. Czyż, Phys. Rev. D **30**, 2371 (1984).
[40] A. Białas and W. Czyż, Z. Phys. C **28**, 255 (1985).
[41] A. Bialas, Nucl. Phys. B **267**, 242 (1986).
[42] M. Gyulassy and A. Iwazaki, Phys. Lett. B **165**, 157 (1985).
[43] G. Gatoff, A. K. Kerman, and T. Matsui, Phys. Rev. D **36**, 114 (1987).
[44] H. T. Elze, M. Gyulassy, and D. Vasak, Nucl. Phys. B **276**, 706 (1986).
[45] H. T. Elze, M. Gyulassy, and D. Vasak, Phys. Lett. B **177**, 402 (1986).
[46] A. Bialas and W. Czyz, Acta Phys. Pol. B **17**, 635 (1986).
[47] W. Florkowski, Acta Phys. Pol. B **35**, 799 (2004).
[48] K. Bajan and W. Florkowski, Acta Phys. Pol. B **32**, 3035 (2001).
[49] A. Bialas, W. Czyz, A. Dyrek, W. Florkowski, and R. B. Peschanski, Phys. Lett. B **229**, 398 (1989).
[50] A. Dyrek and W. Florkowski, Nuovo Cimento A **102**, 1013 (1989).
[51] A. Bialas, W. Czyż, A. Dyrek, and W. Florkowski, Nucl. Phys. B **296**, 611 (1988).
[52] W. Florkowski and R. Ryblewski, Nucl. Phys. A **931**, 343 (2014).
[53] W. Florkowski, *Phenomenology of Ultra-Relativistic Heavy Ion Collisions* (World Scientific, Singapore, 2010), p. 416.
[54] M. Ruggieri, A. Puglisi, L. Oliva, S. Plumari, F. Scardina, and V. Greco, EPJ Web Conf. **117**, 03014 (2016).
[55] V. Voronyuk, V. V. Goloviznin, G. M. Zinovjev, W. Cassing, S. V. Molodtsov, A. M. Snigirev, and V. D. Toneev, Phys. At. Nucl. **78**, 312 (2015), and references therein.
[56] Z. Xu and C. Greiner, Phys. Rev. C **79**, 014904 (2009).
[57] Z. Xu, C. Greiner, and H. Stocker, Phys. Rev. Lett. **101**, 082302 (2008).
[58] E. L. Bratkovskaya, W. Cassing, V. P. Konchakovski, and O. Linnyk, Nucl. Phys. A **856**, 162 (2011).
[59] G. Ferini, M. Colonna, M. Di Toro, and V. Greco, Phys. Lett. B **670**, 325 (2009).
[60] S. Plumari and V. Greco, AIP Conf. Proc. **1422**, 56 (2012).
[61] S. Plumari, A. Puglisi, M. Colonna, F. Scardina, and V. Greco, J. Phys.: Conf. Ser. **420**, 012029 (2013).
[62] S. Plumari, A. Puglisi, F. Scardina, and V. Greco, Phys. Rev. C **86**, 054902 (2012).
[63] M. Ruggieri, F. Scardina, S. Plumari, and V. Greco, Phys. Lett. B **727**, 177 (2013).
[64] M. Ruggieri, F. Scardina, S. Plumari, and V. Greco, Phys. Rev. C **89**, 054914 (2014).
[65] J. C. Maxwell, Philos. Mag. **23**(4), 12 (1861).
[66] G. S. Denicol, U. W. Heinz, M. Martinez, J. Noronha, and M. Strickland, Phys. Rev. D **90**, 125026 (2014).
[67] P. Huovinen and D. Molnar, Phys. Rev. C **79**, 014906 (2009).
[68] A. El, Z. Xu, and C. Greiner, Phys. Rev. C **81**, 041901 (2010).
[69] S. Chapman, Philos. Trans. R. Soc. London A **216**, 279 (1916); **217**, 118 (1917).
[70] M. Ruggieri, S. Plumari, F. Scardina, and V. Greco, Nucl. Phys. A **941**, 201 (2015).
[71] A. Adare *et al.* (PHENIX Collaboration), Phys. Rev. C **91**, 064904 (2015).
[72] J. Adam *et al.* (ALICE Collaboration), Phys. Lett. B **754**, 235 (2016).